BIOCHEMISTRY
including biophysical chemistry & molecular biology

Article

pubs.acs.org/biochemistry

The Structure of the Thioredoxin−Triosephosphate Isomerase Complex Provides Insights into the Reversible Glutathione-Mediated Regulation of Triosephosphate Isomerase

Shahul Hameed M. S. and Siddhartha P. Sarma*

Molecular Biophysics Unit, Indian Institute of Science, Bangalore 560012, Karnataka, India

Supporting Information

ABSTRACT: Protein−protein interactions are crucial for many biological functions. The redox interactome encompasses numerous weak transient interactions in which thioredoxin plays a central role. Proteomic studies have shown that thioredoxin binds to numerous proteins belonging to various cellular processes, including energy metabolism. Thioredoxin has cross talk with other redox mechanisms involving glutathionylation and has functional overlap with glutaredoxin in deglutathionylation reactions. In this study, we have explored the structural and biochemical interactions of thioredoxin with the glycolytic enzyme, triosephosphate isomerase. Nuclear magnetic resonance chemical shift mapping methods and molecular dynamics-based docking have been applied in deriving a structural model of the thioredoxin−triosephosphate isomerase complex. The spatial proximity of active site cysteine residues of thioredoxin to reactive thiol groups on triosephosphate isomerase provides a direct link to the observed deglutathionylation of cysteine 217 in triosephosphate isomerase, thereby reversing the inhibitory effect of S-glutathionylation of triosephosphate isomerase.

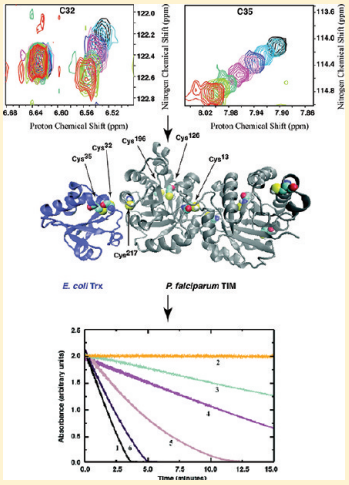

Protein−protein interactions play a very crucial role in a vast majority of physiological processes. This has made protein interactome mapping one of the main foci of current research in an effort to unravel the complex molecular relationships in living systems. Protein−protein interactions can be classified as either permanent or transient on the basis of the lifetime of the protein−protein complex. A complex qualifies as transient if it readily undergoes a change in its oligomeric state. To achieve rapid turnover, protein−protein interactions may be optimized to acquire the ideal lifetime for the molecular function of the protein complex. Examples of such transient complex formation are found among redox proteins. The redox interactome plays a vital role in the regulation of a number of phenomena in the cell that have been linked to the reversible conversion of disulfides to dithiols, thereby modulating the activities of the respective proteins. Proteins belonging to the Trx superfamily are central to the redox interactome, which involves a number of putatively redox-regulated protein targets representing several diverse cellular processes.[1−9] Proteomic studies for identifying Trx targets have unraveled a long list of proteins associated with different cellular processes like energy metabolism, oxidative stress response, transport, amino acid biosynthesis and degradation, DNA metabolism, fatty acid biosynthesis, purine/pyrimidine ribonucleotide biosynthesis, sugar nucleotide metabolism, cell envelope/porins, DNA replication and recombination, protein translation and modification, RNA synthesis, and protein degradation.[2−5] Trx-associated proteins involved in energy metabolism include glycolytic enzymes (enolase, fructose-1,6-bisphosphate aldolase, GAPDH, pyruvate kinase II, and triosephosphate isomerase), the pentosephosphate pathway enzyme (transaldolase B), and TCA cycle enzymes (aconitate hydrase, isocitrate dehydrogenase, succinate dehydrogenase, and succinyl-CoA synthetase).[3−5]

Trx is an important constituent of antioxidant defense against oxidative stress. Oxidative stress has been associated with numerous disease states like atherosclerosis,[10] cancer,[11] malaria,[12] etc., and also age-related degenerative disorders.[13] ROS and RNS play an important role in redox signaling mainly through a set of reversible post-translational modifications, which include S-glutathionylation and S-nitrosylation, of thiol residues in proteins.[14] Several proteins have been shown to be either upregulated or downregulated by S-glutathionylation.[15−17] Glutaredoxins represent the major deglutathionylating redox-active proteins in most living organisms. There are several emerging reports showing Trx constitutes an alternative pathway for protein deglutathionylation.[18] In fact, it has been shown in yeast that Trx serves as the main deglutathionylating redox-active protein.[19] Recent studies have shown evidence of multiple cross talks among Trx, glutaredoxin, and S-glutathionylation targets.[20] There seems to be a high degree of overlap and redundancy among these redox regulators. The enzymes of the glycolytic pathway are usually downregulated by

Received: August 6, 2011
Revised: November 9, 2011
Published: November 29, 2011

S-glutathionylation.[21,22] These enzymes also constitute important targets for dual regulation by glutaredoxin and Trx.[20,23] This is functionally significant in the case of protozoan parasites such as *Plasmodium falciparum*, in which glycolysis is the only functionally intact energy metabolic pathway.[24] The malarial parasites are particularly vulnerable to oxidative stress during the erythrocytic stages of their life cycle, and thiol-based redox systems play a very important role in allowing the parasite to survive in the host under challenging conditions posed by the oxidative burst of the host immune system and endogenous toxic metabolites generated by their own metabolism.[25] In this study, we explore the structural interaction between the glycolytic enzyme TIM and Trx. The structural and enzymatic properties of these two proteins have been studied in great detail. While the interaction between these two proteins has been demonstrated by AP−MS,[3] no information about the structural basis for the interaction is available. The particular TIM[26−31] that we have chosen for this study is from the malarial parasite *P. falciparum*, while the Trx[32,33] used here has its origin in the bacterium *Escherichia coli*. Given the high degree of sequence and structural similarity among the glycolytic enzymes[34] as well as among Trxs[2] across living organisms, it is not unreasonable to expect conservation in the nature of interaction between these proteins as well as conservation in function. Here the structural interactions have been studied by solution NMR spectroscopy. Changes in chemical shift upon complex formation have been used to construct a structural model of the TIM−Trx complex. Functional consequences of this interaction have been elucidated through examination of the enzymatic properties and correlation of these properties with structure. The details of this study are given below.

MATERIALS AND METHODS

Iodoacetic acid (IAA), iodoacetamide (IAM), 5,5′-dithiobis(2-nitrobenzoic acid), bovine trypsin, α-glycerophosphate dehydrogenase, a glyceraldehyde 3-phosphate solution, NADH, amino acids, and $^{15}NH_4Cl$ were purchased from Sigma-Aldrich.

Expression and Purification of PfTIM and Trx. Unlabeled samples of PfTIM and EcTrx were expressed and purified as described previously.[35,36] A purified protein sample of C13E PfTIM was a generous gift from H. Balaram (Jawaharlal Nehru Center for Advanced Scientific Research, Bangalore, India). Samples of EcTrx enriched with ^{15}N were prepared by expressing protein in culture medium in which $^{15}NH_4Cl$ was included as the sole source of nitrogen. Samples of PfTIM with selective unlabeling of amino acids were created by addition of specific amino acids at a concentration of 100 mg/L to the growth medium along with $^{15}NH_4Cl$ as the sole source of nitrogen.[37]

Enzyme Assays. The enzyme activity of PfTIM and C13E PfTIM in the presence and absence of EcTrx was measured according to the protocol suggested by Plaut and Knowles[38] using a Varian CARY 100 double-beam spectrophotometer at room temperature. The assay samples were prepared in 100 mM triethanolamine buffer (pH 7.6) and contained 5 mM EDTA, 0.5 mM NADH, α-glycerophosphate dehydrogenase (20 μg/mL), and 1 mM glyceraldehyde 3-phosphate. An enzyme concentration of 0.5 μg/mL was used for all assays. The enzyme activity was determined by monitoring the decrease in absorbance at 340 nm.

Preparation of Glutathionylated Proteins. Glutathionylation was conducted by incubation of a 20 μM protein solution at physiological temperature (37 °C) for 2 h with 10 mM oxidized glutathione (GSSG). Excess unreacted GSSG was removed by dialysis using microdialysis cassettes at 4 °C.

NMR Titration Studies. *Samples for NMR Spectroscopy.* Purified protein samples were dialyzed against buffer [20 mM phosphate buffer (pH 6.8), 1 mM DTT, and 0.01% NaN_3]. Protein samples were concentrated by ultrafiltration.

NMR Titration Studies of the Interaction of EcTrx with PfTIM. Reduced ^{15}N-labeled Trx protein (0.1 mM) was titrated with unlabeled samples of TIM at concentrations ranging from 0 to 600 μM in a fixed volume of 600 μL. Similarly ^{15}N labeled samples of TIM were titrated with unlabeled samples of reduced Trx using a similar concentration profile. D_2O (10%) was added to all samples prior to the acquisition of NMR data.

Acquisition and Processing of NMR Data. All NMR spectra were recorded at 303 K on Bruker Avance 700 MHz NMR spectrometers using a triple-resonance cryoprobe equipped with a single *Z*-axis pulsed field gradient accessory. Two-dimensional $^1H-^{15}N$ fast HSQC spectra were recorded with labeled samples of Trx using pulse field gradient and a binomial 3-9-19 WATERGATE solvent suppression scheme.[39,40] Data were acquired with 1024 complex t_2 time domain data points and 128 complex t_1 time domain data points. Quadrature detection in t_1 was achieved using the States−TPPI method.[41] Signals in the directly and indirectly detected dimensions were sampled over spectral widths of 12000 and 2128 Hz, respectively. For ^{15}N-labeled samples of PfTIM, SEA-HSQC spectra were recorded to select for those resonances on the surface of the protein that are in exchange with the bulk solvent.[42] All NMR data were processed on an Intel workstation running Suse Linux 11.3 using NMRPipe/NMRDraw processing software.[43] Spectra were processed in both the directly acquired and the indirectly acquired dimensions by applying a squared sine bell weighting function phase-shifted by 90°. Data sets were zero-filled in each dimension to yield spectra with a digital resolution of 1.6 Hz per point in the acquired dimension and 2.1 Hz per point in the indirectly detected dimension. All chemical shifts were referenced to internal water. NMR data were analyzed using ANSIG.[44]

Chemical Shift Mapping. The processed data were analyzed to determine changes in chemical shifts as a function of ligand concentration as observed in the NMR spectra, and shifts were calculated using the equation

$$\Delta = (\Delta\delta_{HN}{}^2 + \Delta\delta_N{}^2)^{1/2} \quad (1)$$

where Δ is the cumulative chemical shift deviation, $\Delta\delta_{HN}$ is the change in the chemical shift of the proton, and $\Delta\delta_N$ is the change in the chemical shift of the nitrogen.[45]

Calculation of Dissociation Constants. Plots of the cumulative chemical shift change versus the concentration of the unlabeled protein were fit to the following equation to yield the dissociation constant, K_d.[45]

$$\Delta\Omega_{obs}/\Delta\Omega_{max} = \{K_d + N_o + R_o - [(K_d + N_o + R_o)^2 - 4R_oN_o]^{1/2}\}/2R_o \quad (2)$$

which was derived from basic formulas

$$K_d = [(R_o - R_N)(N_o - R_N)]/R_N$$

$$R_N = R_o(\Delta\Omega_{obs}/\Delta\Omega_{max})$$

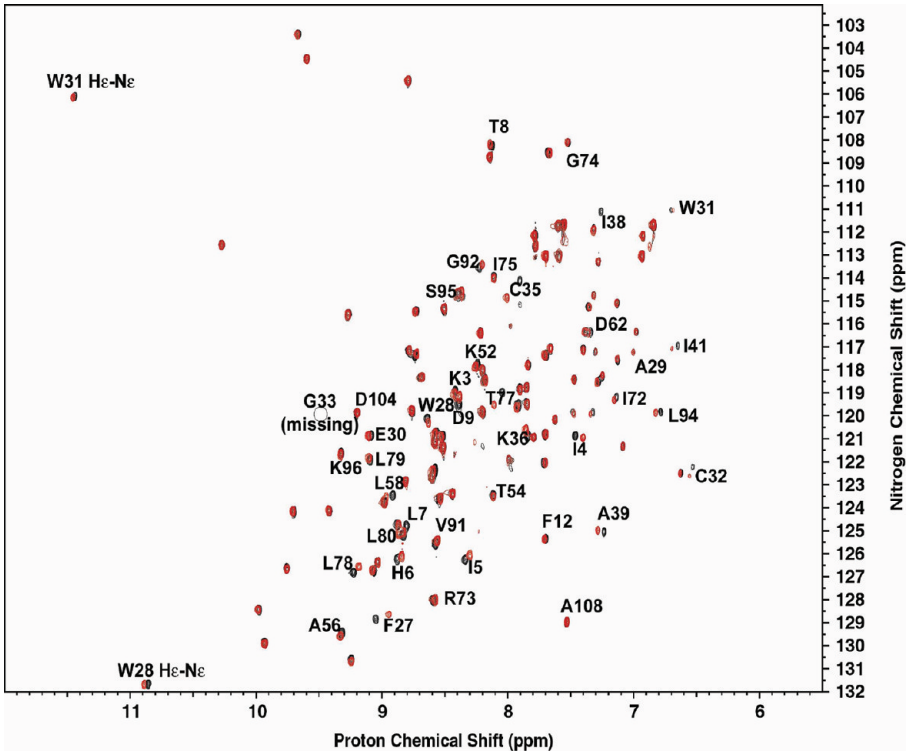

Figure 1. Chemical shift mapping of the binding site of reduced Trx. $^{1}H-^{15}N$ HSQC spectrum of reduced EcTrx upon titration with PfTIM. Black peaks correspond to 0.1 mM free reduced EcTrx and red peaks to 0.1 mM reduced EcTrx titrated with 0.2 mM unlabeled PfTIM.

where Ω_{obs} is the observed chemical shift change at each titration point, Ω_{max} is the maximal observed change during the titration, R_o is the labeled protein concentration (protein), N_o is the unlabeled protein concentration (ligand), R_N is the complex concentration, and the least-squares fitting procedure was performed using MATLAB.

Calculation of the Structure of the PfTIM−EcTrx Complex. Docking of the PfTIM−EcTrx complex was performed using HADDOCK (version 2.1)[46] in combination with CNS.[47] The active and passive residues defined for HADDOCK were chosen on the basis of the chemical shift perturbation data determined above and solvent accessibility calculated using NACCESS. The residues labeled as "active" correspond to all significantly perturbed residues ($\Delta\delta_{bind}$ for ^{1}H of ≥0.030 ppm or for ^{15}N of ≥0.100 ppm) upon complex formation as well as a high solvent accessibility (>50%) in the free form of the protein. The "passive" residues correspond to the residues that are surface neighbors (within 4 Å of the active residues) and have a high solvent accessibility (>50%). An ambiguous interaction restraint (AIR) was defined as an ambiguous intermolecular distance with a maximal value of 3.0 Å between any atom of an active residue of EcTrx and any atom of both active and passive residues of PfTIM.

Docking Protocol. Ensemble docking calculations were performed with five different conformers of reduced EcTrx from the NMR ensemble [Protein Data Bank (PDB) entry 1xob].[48] These five different conformers were chosen on the basis of the highest rmsd across the active site surface area. For PfTIM, the crystal structure (PDB entry 1ydv)[26] was used. Initially, the two partner proteins were positioned 100 Å from each other in space, and each protein was randomly rotated around its center of mass. The two proteins were then docked by rigid body energy minimization, and 1000 rigid-body docking solutions were generated. The best 200 solutions in terms of intermolecular energies were refined using a three-stage semiflexible simulated annealing in torsion angle space. In the first simulated annealing (1000 steps from 2000 to 50 K with 8 fs time steps), the two proteins were considered as rigid bodies and their respective orientation was optimized. In the second simulated annealing (4000 steps from 2000 to 50 K with 4 fs time steps), the side chains at the interface were allowed to move. In the third simulated annealing (1000 steps from 500 to 50 K with 2 fs time steps), both side chains and the backbone at the interface were allowed to move. The resulting structures were then subjected to 200 steps of steepest descent energy minimization. The final stage consists of explicit water refinement in an 8 Å shell of TIP3P water molecules. The system was first heated to 300 K (500 steps at 100, 200, and 300 K) with position restraints on all atoms except for the flexible side chains at the interface. MD steps (5000) were then performed at 300 K with position restraints only on noninterface heavy atoms. During the final cooling stage (1000 MD steps at 300, 200, and 100 K), the position restraints were limited to backbone atoms outside the interface. The final structures were then clustered using the pairwise backbone rmsd at the interface using a 7.5 Å cutoff.

Calculation of the PfTIM−PfTrx structure. A structural model of PfTrx was constructed using the average structure from the NMR ensemble of structures calculated for the reduced form of *Saccharomyces cervesiae* Trx (PDB entry 2I9H).[49] The model was constructed using the web-based program SWISS-MODEL.[50−52] AIR's were then mapped onto the modeled structure of PfTrx on the basis of sequence identity and structural homology. Details of the modeling protocol are described in Supporting Information. The docking protocol described above was applied for the calculation of the structure of the PfTIM−PfTrx complex.

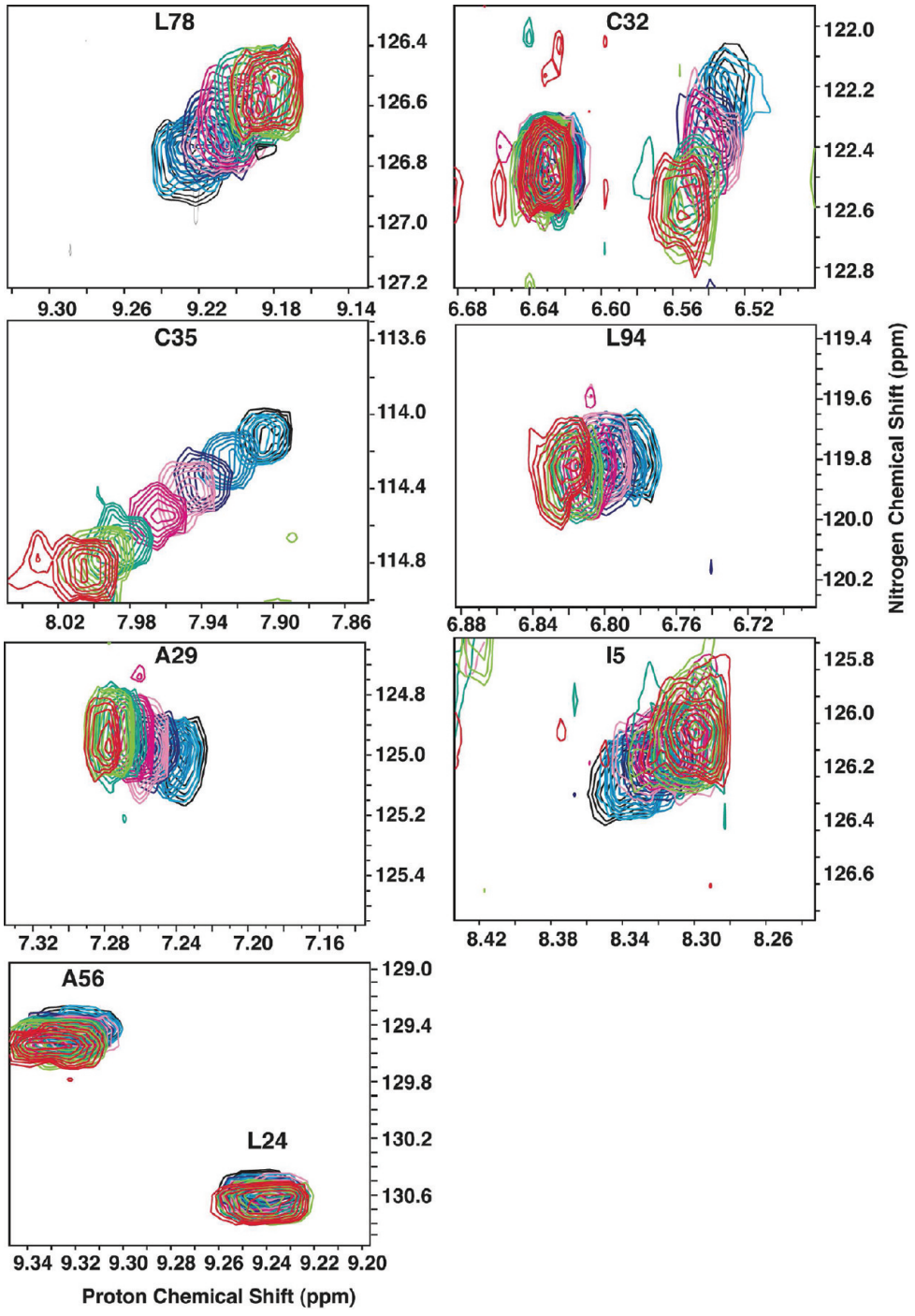

Figure 2. Select regions from overlaid $^{1}H-^{15}N$ HSQC spectra of reduced EcTrx and reduced EcTrx bound to PfTIM. The PfTIM:EcTrx concentration ratios (μM) were 0 (black), 100:100 (pink), and 200:100 (red).

Analysis. The 100 best structures were clustered according to the pairwise rmsd of backbone atoms after alignment of backbone atoms. The rmsd cutoff for clustering was 7.5 Å. Clusters were ranked according to their average interaction energies. We calculated the buried surface area using CNS[47] by taking the difference between the sum of the solvent accessible surface area for each partner separately and the solvent accessible area of the complex. The solvent accessible area was calculated using a 1.4 Å water probe radius. Intermolecular contacts were analyzed using a 3.9 Å heavy-atom distance cutoff for nonbonded contacts. For hydrogen bonds, a distance cutoff of 3.5 Å between donor and acceptor atoms was applied and an angle cutoff of ~120° was used.

RESULTS

Chemical Shift Mapping of EcTrx Titrated with Unlabeled PfTIM. The interaction between PfTIM and EcTrx was monitored by mapping changes in the chemical shift of amide proton−nitrogen resonances of EcTrx as a function of an increasing concentration of PfTIM (Figure 1). A single set of resonances was observed for reduced EcTrx at all titrated concentrations of PfTIM, indicating that the

dx.doi.org/10.1021/bi201224s | *Biochemistry* 2012, 51, 533−544

components of the complex were in fast exchange. Resonance positions in HSQC spectra of amide proton−nitrogen pairs of residues in EcTrx that show significant changes upon binding to PfTIM are shown in Figure 2. Correlation peaks in the $^{1}H-^{15}N$ HSQC spectra correspond to residues whose chemical environments changed as a direct or indirect result of protein−protein interactions. Residues at the active site such as F27, W28 (side chain), W31 (side chain), C32, C35, I38, A39, L78, G92, and L94 experience significant chemical shift perturbations. Residues at the N-terminus, viz., I4, I5, H6, L7, T8, and D9, also experience measurable perturbations that are most likely caused by conformational changes that are induced upon binding. Residues A56 and L24, which lie in the heart of the central β-sheet, and residue A19, which is remote from the active site, are essentially unaffected by the structural interaction between EcTrx and PfTIM.

Mapping the Observed Shifts onto the Structure of Reduced EcTrx. In all, 17 residues exhibited shifts greater than 2.0 Hz. The residues involved in the interaction with PfTIM, when mapped onto the structure of EcTrx, lie as a contiguous stretch on the surface (Figure 3), and this forms the interaction surface on EcTrx.

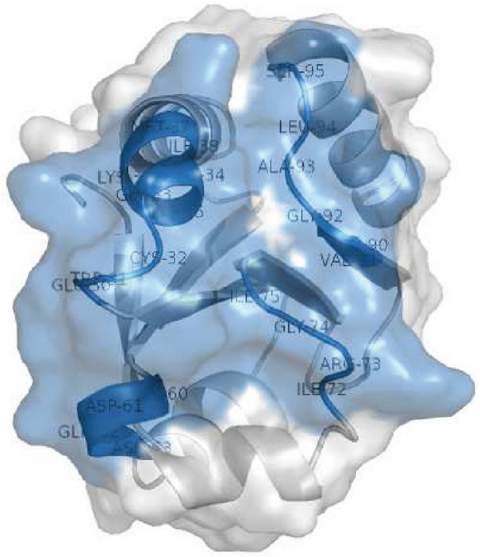

Figure 3. Binding surface of reduced thioredoxin as deduced by chemical shift mapping. Surface residues experiencing chemical shift perturbation during titration with TIM are labeled and colored blue.

Affinity of Interaction. The affinity of interaction was calculated using eq 2. In the fast exchange regime, the observed chemical shifts are population-weighted averages of the two forms of the molecule, viz., the free and bound forms, and thus, fitting of apparent chemical shift curves as a function of added titrant is a function of the dissociation constant, K_d. Figure 4 shows the titration curves for some of the well-resolved and significantly perturbed resonances on EcTrx. Fitting the curves using a 1:1 binding model for the EcTrx−PfTIM interaction yielded a K_d of ~50 μM.

Chemical Shift Mapping of PfTIM Titrated with Unlabeled EcTrx. In a manner analogous to the mapping of chemical shift perturbations in EcTrx upon formation of the complex with PfTIM, here the chemical shift perturbations in PfTIM were also monitored by ^{15}N isotope-edited NMR spectroscopy. It is important to note that chemical shift

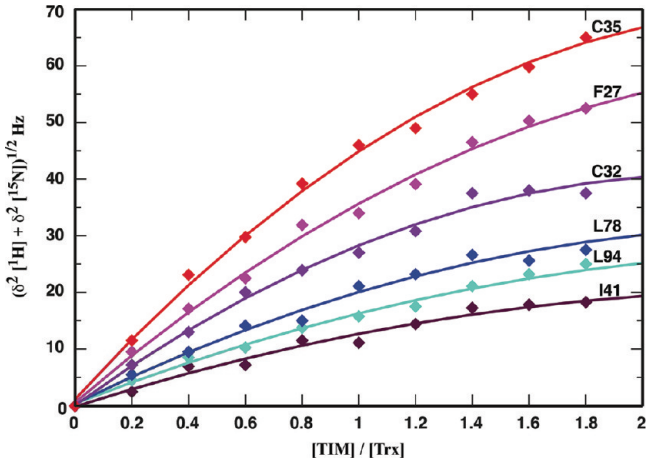

Figure 4. Fitting of the titration curves of well-resolved, significantly perturbed peaks of EcTrx detected in $^{1}H-^{15}N$ HSQC titration experiments. The intrinsic error in the measurement of peak positions is less than 2 Hz.

assignments for PfTIM are not available at present. We have adopted a strategy that involved selective unlabeling schemes followed by selective observation of solvent-exposed amides. Selective unlabeling of residues that are not normally found on the surface of proteins such as isoleucine, leucine, and valine and aromatic amino acids such as phenylalanine, tyrosine, and tryptophan was achieved by incorporation of these amino acids into the growth medium while still providing $^{15}NH_4Cl$ as the sole source of nitrogen. SEA-HSQC spectra of the labeled sample were acquired, and the assignments for backbone amide proton−nitrogen pairs were transferred using the known assignments from yeast TIM.[53] The assignments were then cross-checked with PROSHIFT predictions.[54] Using this strategy, it was observed that residues R3, Q222, E224, D225, and G228 of PfTIM showed significant shifts upon binding with Trx. Figure 5 shows select portions of the SEA-HSQC spectra identifying the shifts observed for the residues listed above.

Determination of the Structure of the EcTrx−PfTIM Docked Complex. *Definition of Ambiguous Interaction Restraints (AIRs).* HADDOCK was used to determine the structure of the docked complex. On the basis of the criteria described in Materials and Methods, residues were labeled as active and passive. In all, 15 and 11 residues were labeled as active in EcTrx and PfTIM, respectively. Similarly, 9 and 4 residues were labeled as passive in EcTrx and PfTIM, respectively. Table 1 lists the identity of these active and passive residues. Using ambiguous interaction restraints, all possible configurations around the interacting site defined by the titration data were searched to find the most favorable pair of interacting amino acids among the active and passive residues. The first stage in the docking protocol consisted of randomization of orientations and rigid body energy minimization to generate 2000 docked complex structures, of which the 200 best solutions in terms of intermolecular energy were refined. The second stage of the docking involved semirigid simulated annealing in torsion angle space (TAD-SA) during which amino acids at the interface (side chains and backbone) were allowed to move to optimize the interface packing. The third and final stage of the docking involved refinement in Cartesian space with explicit solvent. In this stage, although no significant structural changes occur during the

dx.doi.org/10.1021/bi201224s | *Biochemistry* 2012, 51, 533−544

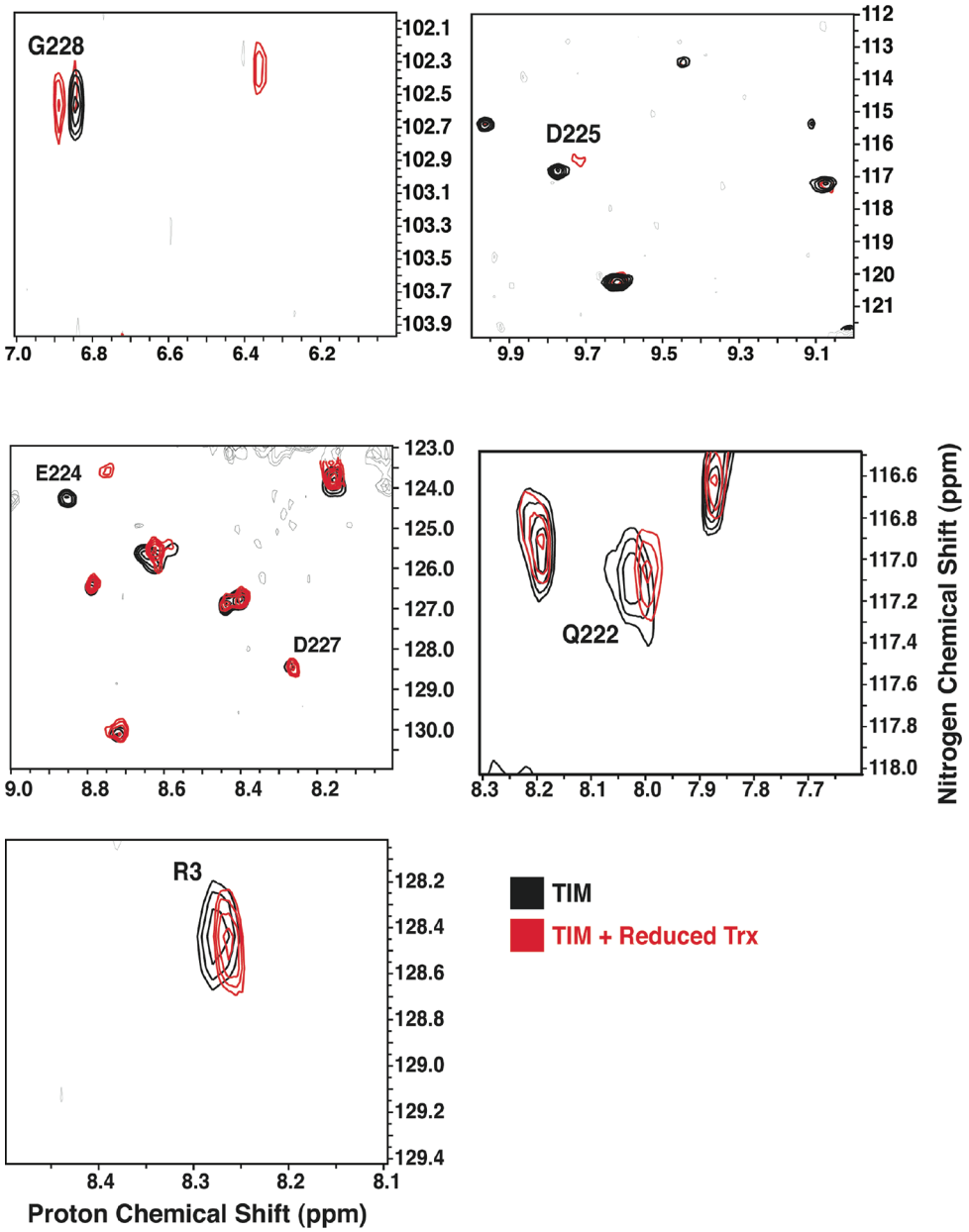

Figure 5. Select regions from overlaid $^{1}H-^{15}N$ SEA HSQC spectra of free PfTIM and EcTrx bound PfTIM. The PfTIM:EcTrx concentration ratios (μM) were 0 (black) and 200:100 (red). The PfTIM used in both cases was selectively unlabeled.

Table 1. Active and Passive Residues Identified in Trx and TIM That Were Used for Docking

reduced Trx	active	E30, W31, C32, C35, K36, M37, I38, D61, Q62, R73, G74, V91, G92, A93, and L94
	passive	W28, A29, A39, I41, L42, Q63, G71, I72, I75, K90, and S95
triosephosphate isomerase	active	R3, K4, K36, Q222, Q223, E224, D225, S246, and M248
	passive	Y5, S35, I221, and I226

water stage, it was useful for the improvement of the energetics of the system. The 100 refined EcTrx–PfTIM complex models, generated by these calculations, were organized in two clusters, with their average rmsd from the lowest-energy structure being 1.14 ± 0.16 and 2.02 ± 0.12 Å when superposed on the N, C^{α}, and C′ backbone atoms. The average intermolecular energy, E_{inter} (sum of intermolecular van der Waals, electrostatic, and AIR energy terms), for the refined structures of the complex in each cluster as well as the structural statistics for the best ranking structure is given in Table 2. For both clusters, the energy term E_{AIR}, which is a measure for the disagreement between calculated structures and experimental restraints, is small (~1 kcal/mol), indicative of a very small number of AIR violations per structure. The average values of buried surface area are in the range of that found in other weak complexes involving EcTrx.

Description of the Calculated Structure of the EcTrx–PfTIM Complex. The resulting model suggests that PfTIM and EcTrx maintain their respective folds after docking. The best structure based on the HADDOCK score is displayed in Figure 6. In the docked complex, it can be seen that residues 3–5 of the N-terminal loop region, residues 31, 35, and 36 of the loop connecting helix 1 with strand 2, a few residues in helix 6, residues in helix 7, and the adjacent loop and residues at the

dx.doi.org/10.1021/bi201224s | *Biochemistry* 2012, 51, 533–544

Table 2. Statistical Analysis of the Two Clusters for the EcTrx−PfTIM Docked Solutions

cluster	no. of structures	E_{inter} (kcal/mol)	E_{vdw} (kcal/mol)	E_{elec} (kcal/mol)	E_{AIR} (kcal/mol)	buried surface area (Å^2)
1	78	−255.9 ± 37.0	−22.8 ± 5.0	−232.5 ± 20.0	1.0 ± 0.7	1237.0 ± 82.0
2	20	−183.7 ± 23.0	−33.5 ± 3.0	−150.2 ± 18.0	0.98 ± 0.3	1160 ± 45.0
Structural Statistics of the Highest-Ranking Docked Model						
no. of ambiguous interaction restraints (AIRs)						
from PfTIM						15
from Trx						24
total AIRs						39
rmsd from idealized covalent geometry						
bonds (Å)						0.0035
angles (deg)						0.5305
impropers (deg)						0.5016
Ramachandran analysis (%)						
residues in the most favored regions						88.6
residues in additionally allowed regions						11.2
residues in generally allowed regions						0.2
residues in disallowed regions						0.0

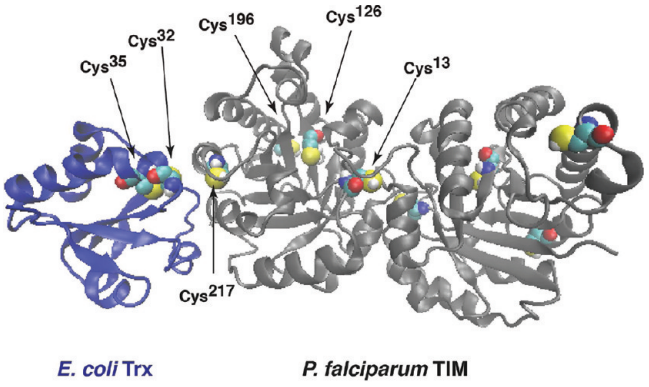

Figure 6. Structural model of the PfTIM−*E. coli* Trx complex. Wild-type PfTIM (dimer) is colored gray and *E. coli* Trx blue.

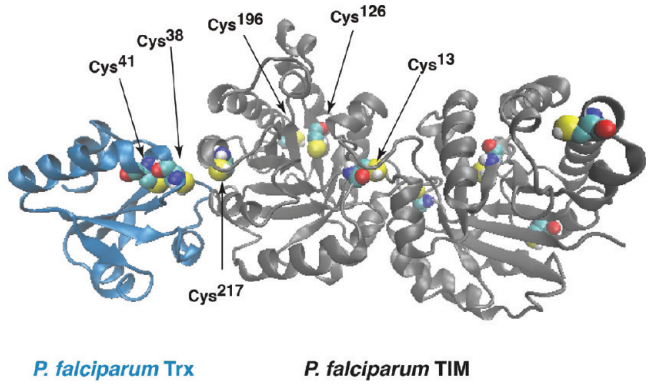

Figure 7. Structural model of the PfTIM−PfTrx complex. Wild-type PfTIM (dimer) is colored gray and *E. coli* Trx blue.

end of the C-terminal helix are all involved in binding. In all, 17 residues (11 from the core and 6 from the rim) from EcTrx and 19 residues (11 from the core and 8 from the rim) form the interface. The surface areas of EcTrx and PfTIM that are buried as a consequence of this interaction are ∼592 and 645 Å^2, respectively.

Intermolecular hydrogen bonding interactions in the top-ranking docked model include the side chain of Lys245 of TIM and the side chain of Asp61 of EcTrx, the amide nitrogen of Met248 of PfTIM and the carbonyl oxygen of Ile72 of EcTrx, and the carbonyl oxygen of Met248 of PfTIM and the amide nitrogen of Ile72 of EcTrx. Nonbonded contacts include the interaction between ring Cε2 of Tyr5 of PfTIM and Cβ of Arg73 of EcTrx, Cβ of Lys245 of PfTIM and ring Cζ2 of Trp31 of EcTrx, Cβ of Met248 and Cβ of Ala67 of EcTrx, Cε of Met248 of PfTIM and Cβ of Ala67 of EcTrx, and the carbonyl carbon of Met248 and the carbonyl carbon of Ile72 of EcTrx.

From the final top-ranking model of the EcTrx−PfTIM complex, a complex of PfTIM with its physiological partner, PfTrx, was created by substitution of *Ec*Trx with a homology model of PfTrx. The system was energy minimized and subjected to molecular dynamics-based energy refinement using HADDOCK. Figure 7 shows a model of the docked PfTrx−PfTIM complex. The PfTrx−PfTIM docked complex had a better energy score and buried surface area than the corresponding complex with *Ec*Trx. The total buried surface area of the PfTrx−PfTIM docked complex was found to be 1485.0 Å^2. The intermolecular hydrogen bonds in the PfTrx−PfTIM docked complex include the following hydrogen bonds: those between the amide nitrogen of Arg3 of PfTIM and the side chain group (Oγ1) of Thr78 of PfTrx, between the side chain nitrogen of Lys36 of PfTIM and the side chain carboxyl group of Glu73 of PfTrx, between the side chain carbonyl group of Gln222 of PfTIM and the amide nitrogen of Met80 of PfTrx, between the side chain of Gln222 of PfTIM and the carbonyl oxygen of Leu96 of PfTrx, between Lys245 of PfTIM and Asp66 of PfTrx, between the amide nitrogen of Met248 of PfTIM and the carbonyl group of Ile77 of PfTrx, between the carbonyl group of Met248 of PfTIM and the side chain of Asn76 of PfTrx, between the carbonyl group of Met248 of PfTIM and the amide nitrogen of Ile77 of PfTrx, and between the terminal carboxyl group of Met248 of PfTIM and the side chain of Asn76 of PfTrx. The residues at the interface in the PfTrx−PfTIM complex are shown in panels A and B of Figure 8.

Comparison of the Trx−TIM Complex with Other Trx−Protein Complexes. The structures of several Trx−protein complexes have been determined to high resolution. Most notable among these are the structures of the T7 DNA polymerase−Trx complex,[55] the Trx−thioredoxin reductase complex,[56] and the ferredoxin−ferredoxin:thioredoxin reductase−Trx ternary complex.[57] The residues of EcTrx that

dx.doi.org/10.1021/bi201224s | *Biochemistry* 2012, 51, 533−544

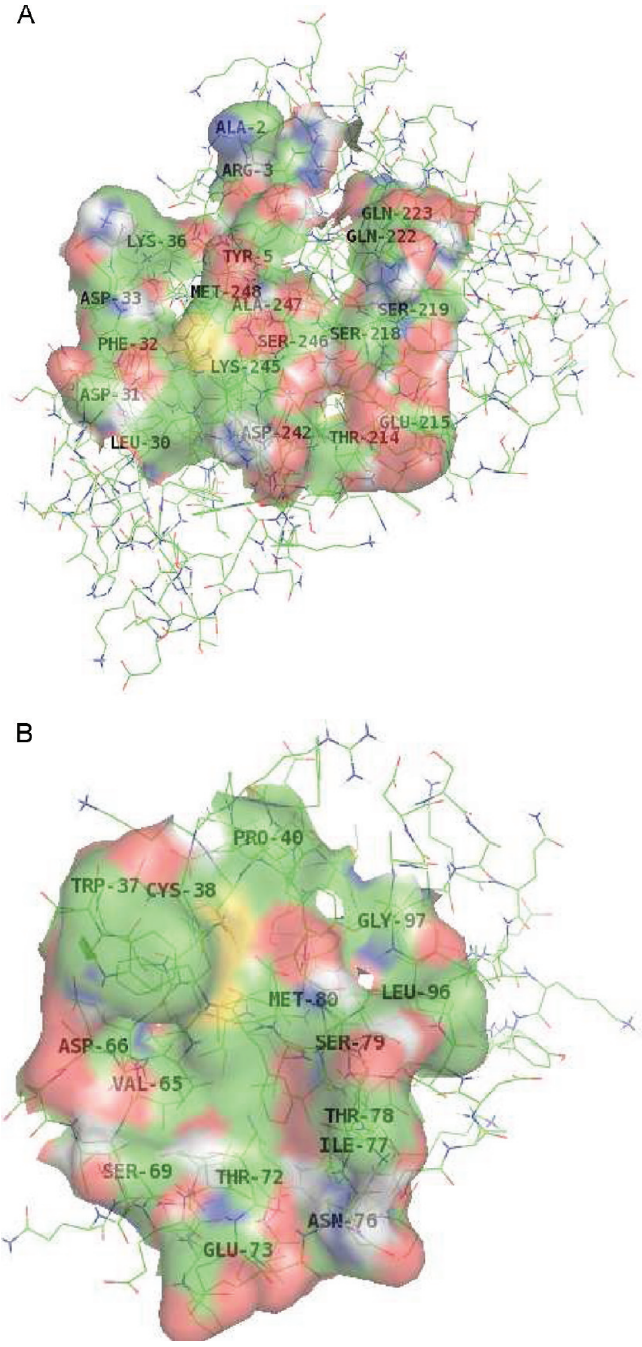

Figure 8. Interface residues of the PfTIM−PfTrx complex. Residues are colored according to their respective polarity, as follows: green for hydrophobic residues, white for nonpolar residues, red for negatively charged residues, and blue for positively charged residues. (A) Interface residues of PfTIM (monomer A) involved in binding with the partner protein as in the docked complex. (B) Interface residues of PfTrx involved in binding with the partner protein as in the docked complex.

participate in the formation of the complex with T7 DNA polymerase, thioredoxin reductase, and PfTIM are listed in Table 3. A strong conservation in the identity of the residues on the binding surface of Trx is apparent, highlighting the fact that the nature of the interaction is similar in all cases.

Enzyme Activity of PfTIM in the Presence of EcTrx. Figure 9 shows the activity of PfTIM in the presence and absence of EcTrx. It is clear that the presence of EcTrx does not cause any

Table 3. Binding Surface Residues of Trx in Different Complexes

partner protein	residues	total IASA (Å^2)	IASA of Trx (Å^2)
T7 DNA polymerase[a]	E30, W31, C32, G33, P34, K36, M37, I60, D61, P64, A67, P68, I72, R73, G74, I75, T89, K90, V91, G92, A93, L94, and Q98	1866	900
thioredoxin reductase[b]	W31, C32, G33, P34, M37, P40, I41, E44, I60, P64, A67, Y70, G71, I72, R73, G74, I75, V91, A93, L94, S95, K96, G97, and Q98	1805	910
TIM[c]	W31, C32, G33, P34, M37, I38, I60, D61, P64, A67, P68, G71, I72, R73, G74, I75, V91, G92, A93, and L94	1350	748

[a]From PDB entry 1T7P.[55] [b]From PDB entry 1TDE.[56] [c]From this study.

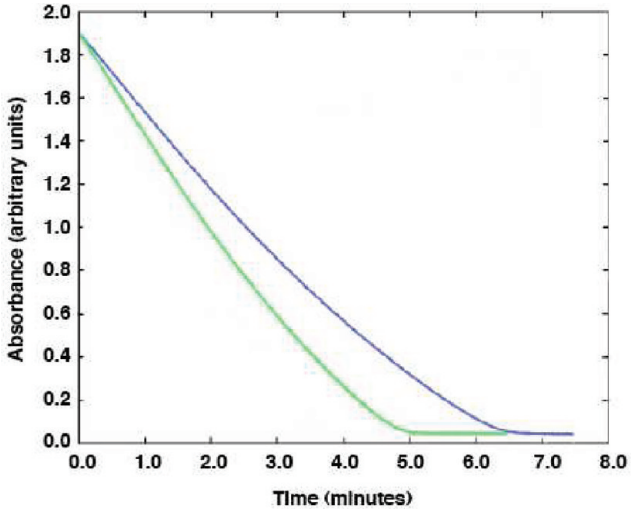

Figure 9. Coupled enzyme assay for PfTIM in the presence of thioredoxin. Colored blue is the kinetic profile of PfTIM, and colored green is the kinetic profile of PfTIM in the presence of 10 μM Trx.

perturbation to the activity of the enzyme. Instead, a modest increase in the reaction rate is observed in the presence of EcTrx.

Deglutathionylation of C13E PfTIM in the Presence of EcTrx. Previously, it has been shown that alkylation of the interface cysteine (Cys13) in PfTIM leads to a loss of enzyme activity.[35] Glutathionylation of the cysteine at position 13 or 217 in PfTIM also leads to a loss of activity. Further, it was found that glutathionylation of Cys217 could be reversed by thiol reducing agents like DTT, leading to enzyme reactivation. However, reactivation of the enzyme by DTT was not possible for PfTIM glutathionylated at Cys13, because like alkylation, glutathionylation of Cys13 also potentially leads to irreversible active site distortion and disruption of the dimer interface. In this study, the deglutathionylating activity of EcTrx on the glutathionylated C13E mutant of PfTIM was probed using a coupled enzyme assay. Incubation of glutathionylated PfTIM and EcTrx restores the activity of the enzyme (Figure 10). The presence of DTT (0.5 mM) helps to maintain EcTrx in the reduced state, where it is active as a deglutathionylating redox-active protein.

dx.doi.org/10.1021/bi201224s | *Biochemistry* 2012, 51, 533−544

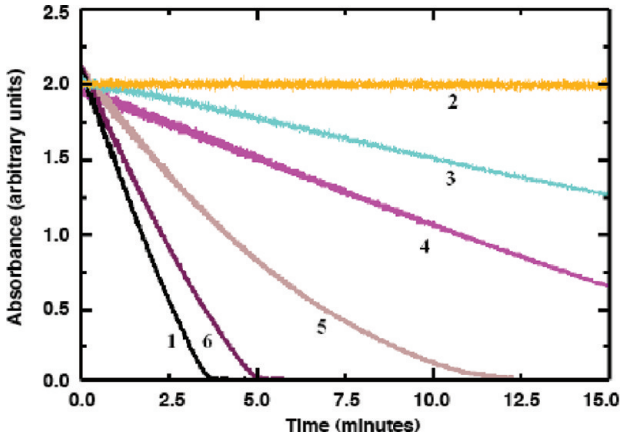

Figure 10. Coupled enzyme assay for C13E PfTIM. Plot 1 shows the kinetic profile of C13E PfTIM. Plot 2 shows the kinetic profile of glutathionylated C13E PfTIM. Plot 3 shows the kinetic profile of glutathionylated C13E PfTIM after incubation with 0.5 mM DTT for 30 min. Plot 4 shows the kinetic profile of glutathionylated C13E PfTIM after incubation with 20 μM Trx and 0.5 mM DTT for 30 min. Plot 5 shows the kinetic profile of glutathionylated C13E PfTIM after incubation with 50 μM Trx and 0.5 mM DTT for 30 min. Plot 6 shows the kinetic profile of glutathionylated C13E PfTIM after incubation with 5 mM DTT.

DISCUSSION

Trx plays a crucial role in maintaining intracellular redox homeostasis. Through its oxidoreductase activity, Trx regulates several cytoplasmic proteins. Under oxidative stress conditions, Trx forms an important constituent of antioxidant defense by acting as a reducing agent for peroxiredoxins that are involved in reduction of hydrogen peroxide and takes part in protein repair by acting as a hydrogen donor for methionine sulfoxide reduction.[58,59] Trx also plays a protective role under conditions of oxidative stress without the involvement of oxidoreductase activity by making complexes with target proteins as in the case of apoptotic signaling kinase, which prevents oxidative stress-triggered apoptosis.[60] Other examples of protein−protein interactions in which Trx functions without the involvement of oxidoreductase activity are those with T7 DNA polymerase and filamentous phage proteins. In both cases, Trx forms tight complexes with the partner proteins.[61−64] In interactions in which Trx modulates the target proteins through its oxidoreductase activity, the interactions are usually transient. Trx reduces the disulfide of the target protein in two fast steps, such that the lifetime of the intermediate complex between Trx and its target is extremely short. Proteomic studies in different organisms across species have shown that Trx interacts with numerous proteins representing several cellular processes, including but not limited to transcription regulation, cell division, energy metabolism, and several biosynthetic pathways. NMR titration studies show that the chemical shift perturbations fall in the fast exchange regime, indicating that the complex formed with TIM is weak and transient. Binding surface mapping using chemical shift perturbations observed during NMR titrations reiterate the fact that Trx employs a consensus binding site for binding target proteins. The consensus binding surface of Trx harbors residues such as Trp, Arg, Tyr, and Ile that have been identified as hot spot residues in a number of other protein−protein interactions.[65] Further, such single-interface hub proteins have been shown to possess rugged bottom binding funnels, which imparts conformational flexibility to sample energetically close multiple conformations.[66−69] The ability of Trx's structurally plastic binding surface to employ a multitude of hot spot residues to varying degrees allows it to form complexes with structurally diverse target proteins with affinities ranging from 10^3 to 10^9 M^{-1}. Determining the structure of weak protein−protein complexes by X-ray crystallography is not possible.[70] Similarly, determining the solution structure of the complex using traditional NOE-based methods is very challenging and less deterministic even after considerable experimental time. Further, this approach needs knowledge of the complete NMR assignments of both unbound and bound components. We have adopted a well-documented strategy in which determined structures of the individual components are docked using experimental chemical shift restraints using a molecular dynamics-based docking method that allows for induced fit and backbone flexibility. The docked TIM−Trx complex seems to provide a physical basis for explaining the deglutathionylating activity of Trx on Cys217-glutathionylated TIM. From the docked complex, it is clear that the active site thiol Cys32 of Trx is close (~6 Å) to Cys217 of PfTIM. We believe that glutathionylation of Cys217 of PfTIM would not drastically alter the binding characteristics of the TIM−Trx complex. From the docked model, the deglutathionylation of TIM by Trx can be explained as follows. Reduced Trx binds noncovalently to TIM, which has been glutathionylated at Cys217, and the nucleophilic thiolate anion of Cys32 of Trx attacks the disulfide sulfur atom of the glutathionylated cysteine at position 217 of PfTIM. This leads to the formation of the so-called mixed disulfide intermediate in which the Trx and the glutathione are covalently bound via a new disulfide bridge. Next, the Cys35 thiol group of the originally reduced Trx is deprotonated. This initiates a thiolate attack of Cys35 on the sulfur atom of Cys32 involved in the disulfide bridge with glutathione, causing cleavage of the latter and the release of the products, i.e., an oxidized Trx and a reduced glutathione. While the deglutathionylating activity of Trx has been shown here, one cannot rule out the role of other redox-active proteins such as glutaredoxin in performing a similar function vis-a-vis regulation of activity of TIM by deglutathionylation of Cys217 of PfTIM. Given the similarity in the overall three-dimensional structure and active site architecture, it is possible that glutaredoxin could perform a similar function. Homologous TIM enzymes that have a conserved cysteine at position 217 like that of human TIM could be potentially redox regulated by glutathionylation and deglutathionylation by Trx superfamily redox-active proteins, and this may have implications in cancer. Further studies of the interaction of glutaredoxin and TIM and studies of the effect of Trx/glutaredoxin on the kinetic properties of TIM will allow us to improve our understanding of the physiological role of this interaction.

CONCLUSIONS

This work reports the first experimental data for the structure of a physiological TIM−Trx complex. The fact that the interface of Trx involved in interaction with TIM seems to be very similar to the binding interface of Trx in other known complexes of Trx reconsolidates the fact that Trx binds to its target proteins using the same binding surface, which is predominantly hydrophobic. The residues in the interface of PfTIM involved in interaction with Trx, including Cys217, seem to have some sequence conservation with some parasite,

plant, and plant fungal pathogens. The docked model of the PfTIM−PfTrx complex determined using NMR chemical shift titration data shows that Cys217 of PfTIM that is buried in the complex is within 6 Å of active site Cys32 of Trx. The fact that deglutathionylation of Cys217 in C13E mutants of PfTIM by reduced EcTrx/DTT can lead to reactivation of enzyme activity functionally validates our docked complex model.

■ ASSOCIATED CONTENT

Supporting Information

A figure showing the sequence alignment and conservation of active site residues in Trxs from different species and the protocol used for generation of the modeled structure of PfTrx. This material is available free of charge via the Internet at http://pubs.acs.org.

■ AUTHOR INFORMATION

Corresponding Author

*Address: 207 Molecular Biophysics Unit, Indian Institute of Science, Bangalore 560012, Karnataka, India. E-mail: sidd@mbu.iisc.ernet.in. Telephone: 918022932839. Fax: 918023600535.

Funding

We thank the Department of Science and Technology and the Department of Biotechnology for the Nuclear Magnetic Resonance and Mass Spectrometric Facilities at the Indian Institute of Science. S.H. is grateful for the doctoral study scholarship from the Indian Institute of Science.

■ ACKNOWLEDGMENTS

S.P.S. thanks Prof. R. Varadarajan (Molecular Biophysics Unit, Indian Institute of Science) and Prof. Hema Balaram (Jawaharlal Nehru Center for Advanced Scientfic Research) for making available the clones for EcTrx and PfTIM, respectively.

■ ABBREVIATIONS

SEA-HSQC, solvent-exposed amide heteronuclear single-quantum coherence; TIM, triosephosphate isomerase; PfTIM, *P. falciparum* triosephosphate isomerase; Trx, thioredoxin; EcTrx, *E. coli* thioredoxin; PfTrx, *P. falciparum* thioredoxin; NMR, nuclear magnetic resonance; HADDOCK, high-ambiguity-driven biomolecular docking; TCA, tricarboxylic acid; AP−MS, affinity tag purification and mass spectrometry; ROS, reactive oxygen species; RNS, reactive nitrogen species; MD, molecular dynamics; NOE, nuclear Overhauser effect; IASA, interface solvent accessible surface; GAPDH, glyceraldehyde-3-phosphate dehydrogenase; rmsd, root-mean-square deviation.

■ REFERENCES

(1) Holmgren, A. (1989) Thioredoxin and glutaredoxin systems. *J. Biol. Chem. 264*, 13963−13966.

(2) Arner, E. S. J., and Holmgren, A. (2000) Physiological functions of thioredoxin and thioredoxin reductase. *Eur. J. Biochem. 267*, 6102−6109.

(3) Kumar, J. K., Tabor, S., and Richardson, C. C. (2004) Proteomic analysis of thioredoxin-targeted protein in *Escherichia coli*. *Proc. Natl. Acad. Sci. U.S.A. 101*, 3759−3764.

(4) Shin-ichiro, K., Takemae, H., Komaki-Yasuda, K., and Kano, S. (2010) Target proteins of the cytosolic thioredoxin in *Plasmodium falciparum*. *Parasitol. Int. 59*, 298−302.

(5) Sturm, N., Jortzik, E., Mailu, B. M., Koncarevic, S., Deponte, M., Forchhammer, K., Rahlfs, S., and Becker, K. (2009) Identification of Proteins Targeted by the Thioredoxin Superfamily in *Plasmodium falciparum*. *PLoS Pathog. 5*, e1000383.

(6) Motohashi, K., Kondoh, A., Stumpp, M. T., and Hisabori, T. (2001) Comprehensive survey of proteins targeted by chloroplast thioredoxin. *Proc. Natl. Acad. Sci. U.S.A. 98*, 11224−11229.

(7) Yamazaki, D., Motohashi, K., Kasama, T., Hara, Y., and Hisabori, T. (2004) Target Proteins of the Cytosolic Thioredoxins in *Arabidopsis thaliana*. *Plant Cell Physiol. 45*, 18−27.

(8) Wong, J. H., Cai, N., Balmer, Y., Tanaka, C. K., Vensel, W. H., Hurkman, W. J., and Buchanan, B. B. (2004) Thioredoxin targets of developing wheat seeds identified by complementary proteomic approaches. *Phytochemistry 65*, 1629−1640.

(9) Hägglund, P., Bunkenborg, J., Yang, F., Harder, L. M., Finnie, C., and Svensson, B. (2010) Identification of thioredoxin target disulfides in proteins released from barley aleurone layers. *J. Proteomics 73*, 1133−1136.

(10) Bonomini, F., Tengattini, S., Fabiano, A., Bianchi, R., and Rezzani, R. (2008) Atherosclerosis and oxidative stress. *Histol. Histopathol. 23*, 381−390.

(11) Halliwell, B. (2007) Oxidative stress and cancer: Have we moved forward? *Biochem. J. 401*, 1−11.

(12) Becker, K., Tilley, L., Vennerstrom, J. L., Roberts, D., Rogerson, S., and Ginsburg, H. (2004) Oxidative stress in malaria parasite-infected erythrocytes: Host−parasite interactions. *Int. J. Parasitol. 34*, 163−189.

(13) Berlett, B. S., and Stadtman, E. R. (1997) Protein Oxidation in Aging, Disease, and Oxidative Stress. *J. Biol. Chem. 272*, 20313−20316.

(14) Di Simplicio, P., Franconi, F., Frosalí, S., and Di Giuseppe, D. (2003) Thiolation and nitrosation of cysteines in biological fluids and cells. *Amino Acids 25*, 333−339.

(15) Dalle-Donne, I., Rossi, R., Giustarini, D., Colombo, R., and Milzani, A. (2007) S-Glutathionylation in protein redox regulation. *Free Radical Biol. Med. 43*, 883−898.

(16) Townsend, D. M. (2007) S-Glutathionylation: Indicator of Cell Stress and Regulator of the Unfolded Protein Response. *Mol. Interventions 7*, 313−324.

(17) Dalle-Donne, I., Rossi, R., Colombo, G., Giustarini, D., and Milzani, A. (2009) Protein S-glutathionylation: A regulatory device from bacteria to humans. *Trends Biochem. Sci. 34*, 85−96.

(18) Bonilla, M., Denicola, A., Marino, S. M., Gladyshev, V. N., and Salinas, G. (2011) Linked Thioredoxin-Glutathione Systems in Platyhelminth Parasites: Alternative Pathways for Glutathione Reduction and Deglutathionylation. *J. Biol. Chem. 286*, 4959−4967.

(19) Greetham, D., Vickerstaff, J., Shenton, D., Perrone, G. G., Dawes, I. W., and Grant, C. M. (2010) Thioredoxins function as deglutathionylase enzymes in the yeast *Sacchromyces cerevisiae*. *BMC Biochem. 11*, 1−10.

(20) Michelet, L., Zaffagnini, M., Massot, V., Keryer, E., Vanacker, H., Miginiac-Maslow, M., Issakidis-Bourguet, E., and Lemaire, S. D. (2006) Thioredoxins, glutaredoxins, and glutathionylation: New crosstalks to explore. *Photosynth. Res. 89*, 225−245.

(21) Ito, H., Iwabuchi, M., and Ogawa, K. (2003) The Sugar-Metabolic Enzymes Aldolase and Triose-Phosphate Isomerase are Targets of Glutathionylation in *Arabidopsis thaliana*: Detection using Biotinylated Glutathione. *Plant Cell Physiol. 44*, 655−660.

(22) Fratelli, M., Demol, H., Puype, M., Casagrande, S., Eberini, I., Salmona, M., Bonetto, V., Mengozzi, M., Duffieux, F., Miclet, E., Bachi, A., Vandekerckhove, J., Gianazza, E., and Ghezzi, P. (2002) Identification by redox proteomics of glutathionylated proteins in oxidatively stressed human T lymphocytes. *Proc. Natl. Acad. Sci. U.S.A. 99*, 3505−3510.

(23) Reichheld, J.-P., Bashandy, T., Siala, W., Riondet, C., Delorme, V., Meyer, A., and Meyer, Y. (2009) Redundancy and Crosstalk Within the Thioredoxin and Glutathione Pathways: A New Development in Plants. *Adv. Bot. Res. 52*, 253−276.

(24) Ginsburg, H. (2010) Malaria parasite stands out. *Nature 466*, 702−703.

(25) Müller, S., Liebau, E., Walter, R. D., and Krauth-Siegel, R. L. (2003) Thiol-based redox metabolism of protozoan parasites. *Trends Parasitol. 19*, 320−328.
(26) Velanker, S. S., Ray, S. S., Gokhale, R. S., Suma, S., Balaram, H., Balaram, P., and Murthy, M. R. (1997) Triosephosphate isomerase from *Plasmodium falciparum*: The crystal structure provides insights into antimalarial drug design. *Structure 5*, 751−761.
(27) Gopal, B., Ray, S. S., Gokhale, R. S., Balaram, H., Murthy, M. R., and Balaram, P. (1999) Cavity-creating mutation at the dimer interface of *Plasmodium falciparum* triosephosphate isomerase: Restoration of stability by disulfide cross-linking of subunits. *Biochemistry 38*, 478−486.
(28) Parthasarathy, S., Balaram, H., Balaram, P., and Murthy, M. R. (2002) Structures of *Plasmodium falciparum* triosephosphate isomerase complexed to substrate analogues: Observation of the catalytic loop in the open conformation in the ligand-bound state. *Acta Crystallogr. D58*, 1992−2000.
(29) Parthasarathy, S., Ravindra, G., Balaram, H., Balaram, P., and Murthy, M. R. (2002) Structure of the *Plasmodium falciparum* triosephosphate isomerase-phosphoglycolate complex in two crystal forms: Characterization of catalytic loop open and closed conformations in the ligand-bound state. *Biochemistry 41*, 13178−13188.
(30) Parthasarathy, S., Eaazhisai, K., Balaram, H., Balaram, P., and Murthy, M. R. (2003) Structure of *Plasmodium falciparum* triosephosphate isomerase-2-phosphoglycerate complex at 1.1-Å resolution. *J. Biol. Chem. 278*, 52461−52470.
(31) Eaazhisai, K., Balaram, H., Balaram, P., and Murthy, M. R. (2004) Structures of unliganded and inhibitor complexes of W168F, a Loop6 hinge mutant of *Plasmodium falciparum* triosephosphate isomerase: Observation of an intermediate position of loop6. *J. Mol. Biol. 343*, 671−684.
(32) Dyson, J. H., Gippert, G. P., Case, D. A., Holmgren, A., and Wright, P. E. (1990) Three-dimensional solution structure of the reduced form of *Escherichia coli* thioredoxin determined by nuclear magnetic resonance spectroscopy. *Biochemistry 29*, 4129−4136.
(33) Katti, S. K., LeMaster, D. M., and Eklund, H. (1990) Crystal structure of thioredoxin from *Escherichia coli* at 1.68 Å resolution. *J. Mol. Biol. 212*, 167−184.
(34) Peregrin-Alvarez, J. M., Tsoka, S., and Ouzounis, C. A. (2003) The Phylogenetic Extent of Metabolic Enzymes and Pathways. *Genome Res. 13*, 422−427.
(35) Maithal, K., Ravindra, G., Balaram, H., and Balaram, P. (2002) Inhibition of *Plasmodium falciparum* triosephosphate isomerase by chemical modification of an interface cysteine: Electrospray ionization mass spectrometric analysis of differential cysteine reactivities. *J. Biol. Chem. 277*, 25106−25114.
(36) Chakrabarti, A., Srivastava, S., Swaninathan, C. P., Surolia, A., and Varadarajan, R. (1999) Thermodynamics of replacing an α-helical Pro residue in the P40S mutant of *E. coli* thioredoxin. *Protein Sci. 8*, 2455−2459.
(37) Vuister, G. W., Kim, S.-J., Wu, C., and Bax, A. (1994) 2D and 3D NMR study of phenylalanine residues in proteins by reverse isotopic labeling. *J. Am. Chem. Soc. 116*, 9206−9210.
(38) Plaut, B., and Knowles, J. R. (1972) pH-dependence of the triose phosphate isomerase reaction. *Biochem. J. 129*, 311−320.
(39) Mori, S., Abeygunawardana, C., Johnson, M. O., and van Zijl, P. C. (1995) Improved sensitivity of HSQC spectra of exchanging protons at short interscan delays using a new fast HSQC (FHSQC) detection scheme that avoids water saturation. *J. Magn. Reson., Ser. B 108*, 94−98.
(40) Piotto, M., Saudek, V., and Sklenar, V. (1992) Gradient-tailored excitation for single-quantum NMR spectroscopy of aqueous solutions. *J. Biomol. NMR 2*, 661−665.
(41) Marion, D., Ikura, M., Tschudin, R., and Bax, A. (1989) Rapid Recording of 2D NMR Spectra without Phase Cycling. Application to the Study of Hydrogen Exchange in Proteins. *J. Magn. Reson. 85*, 393−399.
(42) Lin, D., Sze, K. H., Cui, Y., and Zhu, G. (2002) Clean SEA-HSQC: A method to map solvent exposed amides in large non-deuterated proteins with gradient-enhanced HSQC. *J. Biomol. NMR 23*, 317−322.
(43) Delaglio, F., Grzesiek, S., Vuister, G. W., Zhu, G., Pfeifer, J., and Bax, A. (1995) NMRPipe: A multidimensional spectral processing system based on UNIX pipes. *J. Biomol. NMR 6*, 277−293.
(44) Kraulis, P. J., Domaille, P. J., Campbell-Burk, S. L., van Aken, T., and Laue, E. D. (1994) Solution Structure and Dynamics of Ras p21.GDP Determined by Heteronuclear Three- and Four-Dimensional NMR Spectroscopy. *Biochemistry 33*, 3515−3531.
(45) Cavanagh, J., Fairbrother, W. J., Palmer, A. G., III, Rance, M., and Skelton, N. J. (2007) *Protein NMR Spectroscopy: Principles and Practice*, 2nd ed., Academic Press, New York.
(46) Dominguez, C., Boelens, R., and Bonvin, A. M. (2003) HADDOCK: A protein-protein docking approach based on biochemical and/or biophysical information. *J. Am. Chem. Soc. 125*, 1731−1737.
(47) Brunger, A. T., Adams, P. D., Clore, G. M., DeLano, W. L., Gros, P., Grosse-Knutsleve, R. W., Jiang, J.-S., Kuszewski, J., Pannu, N. S., Read, R. J., Rice, L. M., Simonson, T., and Warren, G. L. (1998) Crystallography & NMR System. *Acta Crystallogr. D54*, 905−921.
(48) Jeng, M. F., Campbell, A. P., Begley, T., Holmgren, A., Case, D. A., Wright, P. E., and Dyson, H. J. (1994) High-resolution solution structures of oxidized and reduced *Escherichia coli* thioredoxin. *Structure 2*, 853−868.
(49) Sá Pinheiro, A., Cardoso Amorim, G., Soares Netto, L. E., Almeida, F. C. L., and Paula Valente, A. (2008) NMR solution structure of the reduced form of thioredoxin 1 from *Sacharomyces cerevisiae*. *Proteins 70*, 584−587.
(50) Arnold, K., Bordoli, L., Kopp, J., and Schwede, T. (2006) The SWISS-MODEL Workspace: A web-based environment for protein structure homology modelling. *Bioinformatics 22*, 195−201.
(51) Kiefer, F., Arnold, K., Künzli, M., Bordoli, L., and Schwede, T. (2009) The SWISS-MODEL Repository and associated resources. *Nucleic Acids Res. 37*, D387−D392.
(52) Peitsch, M. C. (1995) Protein modeling by E-mail. *Bio/Technology 13*, 658−660.
(53) Loria, J. P., Chunyu, W., Francesca, M., Rance, M., and Palmer, A. G., III (2011) Backbone ^{1}H, ^{13}C, and ^{15}N Chemical Shift Assignments for yeast triosephosphate isomerase, TIM. BMRB entry 7216.
(54) Meiler, J. (2003) PROSHIFT: Protein chemical shift prediction using artificial neural networks. *J. Biomol. NMR 26*, 25−37.
(55) Doublie, S., Tabor, S., Long, A. M., Richardson, C. C., and Ellenberger, T. (1998) Crystal structure of a bacteriophage T7 DNA replication complex at 2.2 Å resolution. *Nature 391*, 251−258.
(56) Waksman, G., Krishna, T. S. R., Williams, C. H. Jr., and Kuriyan, J. (1994) Crystal structure of *Escherichia coli* thioredoxin reductase refined at 2 Å resolution. Implications for a large conformational change during catalysis. *J. Mol. Biol. 236*, 800−816.
(57) Xu, X., Schrmann, P., Chung, J.-S., Hass, M. A. S., Kim, S.-K., Hirasawa, M., Tripathy, J. N., Knaff, D. B., and Ubbink, M. (2009) Ternary Protein Complex of Ferredoxin, Ferredoxin:Thioredoxin Reductase, and Thioredoxin Studied by Paramagnetic NMR Spectroscopy. *J. Am. Chem. Soc. 131*, 17576−17582.
(58) Won Kang, S., Zoon Chae, H., Seok Seo, M., Kim, K., Baines, I. C., and Rhee, S. G. (1998) Mammalian Peroxiredoxin Isoforms Can Reduce Hydrogen Peroxide Generated in Response to Growth Factors and Tumor Necrosis Factor-α. *J. Biol. Chem. 273*, 6297−6302.
(59) Zoon Chae, H., Won Kang, S., and Rhee, S. G. (1999) Isoforms of mammalian peroxiredoxin that reduce peroxides in presence of thioredoxin. *Methods Enzymol. 300*, 219−226.
(60) Zhang, P., Liu, B., Won Kang, S., Seok Seo, M., Rhee, S. G., and Obeid, L. M. (1997) Thioredoxin Peroxidase Is a Novel Inhibitor of Apoptosis with a Mechanism Distinct from That of Bcl-2. *J. Biol. Chem. 272*, 30615−30618.

(61) Mark, D. F., and Richardson, C. C. (1976) *Escherichia coli* thioredoxin: A subunit of bacteriophage T7 DNA polymerase. *Proc. Natl. Acad. Sci. U.S.A. 73*, 780−784.
(62) Bedford, E., Tabor, S., and Richardson, C. C. (1997) The thioredoxin binding domain of bacteriophage T7 DNA polymerase confers processivity on *Escherichia coli* DNA polymerase I. *Proc. Natl. Acad. Sci. U.S.A. 94*, 479−484.
(63) Russel, M., and Model, P. (1985) Thioredoxin is required for filamentous phage assembly. *Proc. Natl. Acad. Sci. U.S.A. 82*, 29−33.
(64) Russel, M., and Model, P. (1986) The role of thioredoxin in filamentous phage assembly. Construction, isolation, and characterization of mutant thioredoxins. *J. Biol. Chem. 261*, 14997−15005.
(65) Moreira, I. S., Fernandes, P. A., and Ramos, M. J. (2007) Hot Spots: A Review of the Protein-protein Interface Determinant Amino-acid Residues. *Proteins 68*, 803−812.
(66) Erijman, A., Aizner, Y., and Shifman, J. M. (2011) Multispecific Recognition: Mechanism, Evolution, and Design. *Biochemistry 50*, 602−611.
(67) Patil, A., Kinoshita, K., and Nakamura, H. (2010) Hub Promiscuity in Protein-Protein Interaction Networks. *Int. J. Mol. Sci. 11*, 1930−1943.
(68) Tsai, C.-J., Kumar, S., Ma, B., and Nussinov, R. (1999) Folding funnels, binding funnels, and protein function. *Protein Sci. 8*, 1181−1190.
(69) Ma, B., Kumar, S., Tsai, C.-J., and Nussinov, R. (1999) Folding funnels and binding mechanisms. *Protein Eng. 12*, 713−720.
(70) Krissinel, E. (2011) Macromolecular complexes in crystals and solutions. *Acta Crystallogr. D67*, 376−385.